






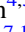







Consistency of the Parkes Pulsar Timing Array Signal with a Nanohertz Gravitational-wave Background

Boris Goncharov^{1,2} , Eric Thrane^{3,4} , Ryan M. Shannon^{4,5} , Jan Harms^{1,2} , N. D. Ramesh Bhat⁶ , George Hobbs⁷,
Matthew Kerr⁸ , Richard N. Manchester⁷ , Daniel J. Reardon^{4,5} , Christopher J. Russell⁹ , Xing-Jiang Zhu¹⁰ , and
Andrew Zic^{7,11} 

¹ Gran Sasso Science Institute (GSSI), I-67100 L'Aquila, Italy; boris.goncharov@me.com

² INFN, Laboratori Nazionali del Gran Sasso, I-67100 Assergi, Italy

³ School of Physics and Astronomy, Monash University, Clayton, VIC 3800, Australia

⁴ ARC Centre of Excellence for Gravitational Wave Discovery, Australia

⁵ Centre for Astrophysics and Supercomputing, Swinburne University of Technology, PO Box 218, Hawthorn, VIC 3122, Australia

⁶ International Centre for Radio Astronomy Research, Curtin University, Bentley, WA 6102, Australia

⁷ Australia Telescope National Facility, CSIRO, Space and Astronomy, PO Box 76, Epping, NSW 1710, Australia

⁸ Space Science Division, Naval Research Laboratory, Washington, DC 20375-5352, USA

⁹ CSIRO Scientific Computing, Australian Technology Park, Locked Bag 9013, Alexandria, NSW 1435, Australia

¹⁰ Advanced Institute of Natural Sciences, Beijing Normal University, Zhuhai 519087, People's Republic of China

¹¹ School of Mathematical and Physical Sciences, and Research Centre in Astronomy, Astrophysics and Astrophotonics, Macquarie University, NSW 2109, Australia

Received 2022 April 11; revised 2022 May 27; accepted 2022 June 8; published 2022 June 17

Abstract

Pulsar timing array experiments have recently reported strong evidence for a common-spectrum stochastic process with a strain spectral index consistent with that expected of a nanohertz-frequency gravitational-wave background, but with negligible yet non-zero evidence for spatial correlations required for a definitive detection. However, it was pointed out by the Parkes Pulsar Timing Array (PPTA) collaboration that the same models used in recent analyses resulted in strong evidence for a common-spectrum process in simulations where none is present. In this work, we introduce a methodology to distinguish pulsar power spectra with the same amplitude from noise power spectra of similar but distinct amplitudes. The former is the signature of a spatially uncorrelated pulsar term of a nanohertz gravitational-wave background, whereas the latter could represent ensemble pulsar noise properties. We test the methodology on simulated data sets. We find that the reported common process in PPTA pulsars is indeed consistent with the spectral feature of a pulsar term. We recommend this methodology as one of the validity tests that the real astrophysical and cosmological backgrounds should pass, as well as for inferences about the spatially uncorrelated component of the background.

Unified Astronomy Thesaurus concepts: [Gravitational waves \(678\)](#); [Millisecond pulsars \(1062\)](#); [Pulsar timing method \(1305\)](#); [Astronomy data analysis \(1858\)](#); [Bayesian statistics \(1900\)](#); [Importance sampling \(1892\)](#); [Supermassive black holes \(1663\)](#); [Gravitational wave astronomy \(675\)](#); [Hierarchical models \(1925\)](#); [High energy astrophysics \(739\)](#); [Astronomical methods \(1043\)](#)

1. Introduction

Pulsar timing array (PTA) experiments pursue the goal of detecting nanohertz-frequency gravitational waves through temporal and spatial cross-correlation of pulse arrival times from millisecond radio pulsars. The primary target sources of such signals are coalescing supermassive binary black holes separated by less than ~ 0.1 pc. Nanohertz gravitational waves produce correlations in the timing residuals between the measured arrival times and the arrival times predicted by the deterministic pulsar timing models (Edwards et al. 2006). Recent searches for the stochastic gravitational-wave background by NANOGrav¹² (Arzoumanian et al. 2020), PPTA¹³

(Goncharov et al. 2021a), EPTA¹⁴ (Chen et al. 2021), and IPTA¹⁵ (Antoniadis et al. 2022) reported evidence for the “common-spectrum process”, the same power-law component in Fourier spectra of timing residuals. The spatial correlations necessary to claim a detection originate from the so-called Earth term of the gravitational-wave background (Hellings & Downs 1983). The pulsar term of the background arises from the passage of gravitational waves near the pulsars and only manifests as a spatially uncorrelated process with the same spectrum of temporal correlations in all of the pulsars. It is expected that evidence for the common-spectrum process, to which both of the terms contribute, would precede the detection of the gravitational-wave background (Pol et al. 2021; Romano et al. 2021). Goncharov et al. (2021a), on the other hand, pointed out that the methodology employed by Arzoumanian et al. (2020) does not allow us to distinguish between common and similar noise processes in pulsars. So, it is unclear if

¹² The North American Nanohertz Observatory for Gravitational Waves (McLaughlin 2013).

¹³ The Parkes Pulsar Timing Array (Manchester et al. 2013).



Original content from this work may be used under the terms of the [Creative Commons Attribution 4.0 licence](#). Any further distribution of this work must maintain attribution to the author(s) and the title of the work, journal citation and DOI.

¹⁴ The European Pulsar Timing Array (Desvignes et al. 2016).

¹⁵ The International Pulsar Timing Array (Verbiest et al. 2016), a consortium of all pulsar timing arrays across the world.

recent searches have detected a bona fide gravitational-wave background.

One might ask why do we need to precisely determine the degree of similarity in pulsar spectra if the detection mostly depends on spatial correlations anyway? There are several reasons. Noise processes with similar and not common noise spectra could arise from, e.g., spin noise, stochastic irregularities in the rotation of the pulsars (Shannon & Cordes 2010). In fact, the spin noise model discussed in Meyers et al. (2021) suggests a spectral index of timing residuals to be $\gamma = 4$ (where the power spectral density is modeled as $P(f) \propto f^{-\gamma}$), which would be difficult to distinguish from the nanohertz gravitational-wave background expected from binary supermassive black holes, $\gamma = 13/3$, with current PTAs (see e.g., Figure 13 in Renzini et al. 2022, to inspect measurement uncertainties). Empirical models for spin noise in millisecond pulsars predict timing noise having spectral indices and amplitudes similar to that expected of the gravitational-wave background. If the reported signal in PTAs is not common and thus not of a gravitational-wave origin, it could have interesting implications for spin noise and hence for neutron star physics (Melatos & Link 2014). Furthermore, the amplitude of the common-spectrum process is in tension with several predictions for the stochastic background amplitude. Recent work by Izquierdo-Villalba et al. (2022) suggests that the gravitational-wave background of the same strain amplitude as the common-spectrum process is challenging to produce in theory given the constraints from the quasar bolometric luminosity functions or the local black hole mass function. Casey-Clyde et al. (2022) find the local number density of supermassive binary black holes inferred from the amplitude of the common-spectrum process, assuming it to originate from the stochastic background, to be five times larger than theoretical predictions. So, even if PTAs are observing hints of a gravitational-wave background, inferences based on the common-spectrum process might be contaminated by pulsar-intrinsic noise, and it is important to clarify to what degree it is true. Such inferences can be promising because the constraints on the background amplitude from interpulsar correlations lag behind the ones based on spatial autocorrelations for most pulsar timing arrays (Pol et al. 2021).

Whereas previous analyses of time-correlated noise in pulsars were based on identifying (e.g., Lentati et al. 2016; Goncharov et al. 2021b) or modeling (Caballero et al. 2016; Goncharov et al. 2020; Chalumeau et al. 2022) noise power spectra, here we focus on modeling Bayesian priors using the second PPTA data release (PPTA DR2; Kerr et al. 2020). The methodology is described in Section 2. In Section 3 we outline the results and we summarize the conclusions in Section 4.

2. Methodology

2.1. Inference of the Common-spectrum Process

The timing residuals comprise a number of stochastic processes. Those that are not due to gravitational waves are considered noise. Temporally correlated processes are called red, whereas processes without temporal correlations are referred to as white. The power spectral density of red processes is usually assumed to be a power law:

$$P(f|A, \gamma) = \frac{A^2}{12\pi^2} \left(\frac{f}{\text{yr}^{-1}} \right)^{-\gamma} \text{yr}^3, \quad (1)$$

where the amplitude A is in the units of strain amplitude of the stochastic gravitational-wave background at $f = \text{yr}^{-1}$ and $-\gamma$ is a spectral index. The frequency in Fourier spectra of fluctuations in timing residuals and concurrently a frequency of a gravitational wave that would have induced these fluctuations are denoted f . To clarify, for white noise, P is a constant; it does not depend on f . Red-process spectra are modeled at n_c harmonically related frequencies that are multiples of the reciprocal of the observation span. Values of n_c , as well as priors for A and γ , and the list of noise terms found in PPTA DR2 were published in Goncharov et al. (2021a). Additional details on the noise models in PPTA DR2 are outlined by Goncharov et al. (2021b). All noise, timing model parameters, and signals of interest are modeled using the multivariate Gaussian likelihood (Lentati et al. 2014; Arzoumanian et al. 2016; Taylor et al. 2017) and Bayesian posterior sampling. Without accounting for spatial correlations, the total PTA likelihood is a product of individual pulsar likelihoods. In particular, for a common-spectrum process with A_c and γ_c , the total PTA likelihood is

$$\mathcal{L}(\mathbf{d}|\boldsymbol{\theta}, A_c, \gamma_c) = \prod_{k=1}^N \mathcal{L}(\mathbf{d}_k|\boldsymbol{\theta}_k, A_c, \gamma_c), \quad (2)$$

where $\boldsymbol{\theta} = (\boldsymbol{\theta}_1, \dots, \boldsymbol{\theta}_N)$ are parameters of models that describe data of individual pulsars $\mathbf{d} = (\mathbf{d}_1, \dots, \mathbf{d}_N)$, including the pulsar-intrinsic “spin” noise parameters A_k, γ_k and parameters of other noise terms that are not of interest to us for the purpose of this work. Some of these parameters are marginalized over analytically (van Haasteren et al. 2009) and others numerically,¹⁶ so $\boldsymbol{\theta}$ is omitted from the following equations. Both for the common-spectrum process found in PPTA DR2 and for a classical model of the stochastic gravitational-wave background from circular supermassive black hole binaries, $\gamma_c = 13/3$. We will fix γ_c at this value throughout our analysis. We provide additional remarks on the data and analysis in Appendix A.

2.2. Importance Sampling for Pulsar Timing Arrays

When it is computationally challenging to evaluate a likelihood or to include several measurements in one likelihood, many data analyses resort to the so-called importance sampling (Ch. 10 in Gelman et al. 1995; Payne et al. 2019). The idea is that the analysis is first carried out assuming a proposal distribution—a likelihood or a prior that is easy to evaluate. Next, posterior samples obtained from this first step are used to evaluate the target distribution—a likelihood or a prior that represents the model we are ultimately interested in. Finally, if proposal samples are collected from subsets of a total data set, they can be combined into a single likelihood through the procedure known as posterior recycling (Thrane & Talbot 2019). To sum up, importance sampling revolves around the reweighing of likelihoods and priors.

Let us represent our signal likelihood given by Equation (2) through target likelihoods with the common-spectrum process, $\mathcal{L}(\mathbf{d}_k|A_{k,j}, \gamma_{k,j}, A_c, \gamma_c)$, and the proposal likelihood without the

¹⁶ These parameters are fit for but not presented in our results. Posterior samples for $\boldsymbol{\theta}_k$ are reweighted in target and proposal likelihoods, and the total likelihood is generally independent of them unless otherwise specified.

common-spectrum process, $\mathcal{L}(d_k|A_{k,j}, \gamma_{k,j})$. Both the proposal and the target likelihoods will represent individual pulsars, whereas the total signal likelihood includes contributions from all pulsars:

$$\mathcal{L}(\mathbf{d}|A_c) = \prod_k^N \mathcal{Z}(d_k) \frac{1}{n_k} \sum_{j=1}^{n_k} \frac{\mathcal{L}(d_k|A_{k,j}, \gamma_{k,j}, A_c)}{\mathcal{L}(d_k|A_{k,j}, \gamma_{k,j})}. \quad (3)$$

Here, the sum is over the n_k fiducial posterior samples j for pulsar k , generated for the proposal distribution. The product is over pulsars. The posterior samples include (A_k, γ_k) , the amplitude, and the spectral index of the red noise for pulsar k . We use these fiducial samples as the ‘‘proposal distribution’’ in order to explore a more complicated likelihood (the ‘‘target distribution’’). The Bayesian evidence $\mathcal{Z}(d_k)$ is the integral of the (proposal) likelihood over the prior. Importance sampling is similar to the factorized likelihood approach (Taylor et al. 2022), where the amplitude of the common-spectrum process is obtained through the multiplication of posterior distributions obtained in analyses of individual pulsar data.

2.3. Common versus Quasi-common

In the case of a common-spectrum process, which could originate from the gravitational-wave background, nature provides us with one A_c in all pulsars. In the language of hierarchical Bayesian statistics (Chapter 5 in Gelman et al. 1995), $A_{c,k}$ for a pulsar k is drawn from a delta function distribution, described by a hyperparameter that determines the position of a delta function distribution along possible values of A_c . The standard null hypothesis is that there is no common-spectrum process and pulsar data sets are described by individual pulsar noise. In this work, we propose an alternative null hypothesis where $A_{c,k}$ are drawn from a Gaussian distribution described by the hyperparameters σ_A, μ_A and not from the delta function distribution described by A_c . So, in Equation (3), we introduce multiple possible values of $A_{c,k}$ and marginalize over the likelihood of such a noise process over the Gaussian¹⁷ prior $\pi(A_{q,c,k}|\mu_A, \sigma_A)$ with hyperparameters μ_A and σ_A being the mean and the standard deviation of the Gaussian prior, respectively,

$$\mathcal{L}(\mathbf{d}|\mu_A, \sigma_A) = \prod_k^N \mathcal{Z}(d_k) \frac{1}{n_k} \sum_{j=1}^{n_k} \frac{\int \mathcal{L}(d_k|A_{k,j}, \gamma_{k,j}, A_{q,c,k}) \pi(A_{q,c,k}|\mu_A, \sigma_A) dA_{q,c,k}}{\mathcal{L}(d_k|A_{k,j}, \gamma_{k,j}, A_{q,c,k})}. \quad (4)$$

We provide a derivation in Appendix C. For $\sigma_A = 0$, $\pi(A_{q,c,k}|\mu_A, \sigma_A)$ reduces to the delta function. Therefore, the likelihood $\mathcal{L}(\mathbf{d}|A_c)$ in Equation (3) is a subset of the likelihood $\mathcal{L}(\mathbf{d}|\mu_A, \sigma_A)$ in Equation (4). We refer to noise processes with $\sigma_A \neq 0$ as quasi-common, which means that noise spectra in timing array pulsars are similar but not common. The measurement of σ_A and μ_A described in this section is also applicable to modeling pulsar spin noise alone, which is broadly distributed in A_k . Instead, here we only infer parameters on the second common term A_{qc} to map the

measurements directly to the result of the gravitational-wave search with PPTA DR2 (Goncharov et al. 2021a). The principle of the quasi-common noise model is similar to the dropout analysis (see Figure 9 in Arzoumanian et al. 2020); it quantifies how constraints on the common-spectrum process with one of the pulsars are consistent with constraints from the rest of the pulsars. As Bayes factors, high dropout factors for pulsars support the common-spectrum process, whereas low dropout factors that approach zero illuminate pulsars that do not have the same spectra as the others.

We calculate the integral over $A_{q,c,k}$ for every evaluation of the likelihood $\mathcal{L}(\mathbf{d}|\mu_A, \sigma_A)$ in Equation (4) the following way. First, we precompute $\mathcal{L}(d_k|A_{k,j}, \gamma_{k,j}, A_{q,c,k})$ on a grid of $A_{q,c,k}$ for n_k posterior samples for N pulsars. Next, for every parameter sample (μ_A, σ_A) , we evaluate the prior for the grid of $A_{q,c,k}$, multiply it by the precomputed likelihood $\mathcal{L}(d_k|A_{k,j}, \gamma_{k,j}, A_{q,c,k})$, and evaluate the integral over the product numerically. Because parameter estimation is traditionally performed on the (base-10) logarithm of the red-process amplitude, in practice we measure $\mu_{\log_{10}A}$ and $\sigma_{\log_{10}A}$ instead of μ_A and σ_A .

3. Results

We measure $\mu_{\log_{10}A}$ and $\sigma_{\log_{10}A}$ in PPTA DR2 (Kerr et al. 2020), with a particular emphasis on $\sigma_{\log_{10}A}$, which distinguishes a common-spectrum process from a quasi-common noise process, as pointed out in Section 2.3. We find Savage-Dickey (1971) natural log Bayes factor in favor of $\sigma_{\log_{10}A} = 0$ against other $\sigma_{\log_{10}A}$ within the uniform prior to be -0.16 . This means that $\sigma_{\log_{10}A}$ is consistent with zero. We further calculate an upper limit on $\sigma_{\log_{10}A} < 0.44$ at 95% credibility. Thus, we demonstrate that the data are more consistent with a common-spectrum-process hypothesis than the extended quasi-common-process model. We measure $\mu_{\log_{10}A} = -14.71^{+0.08}_{-0.14}$, which is consistent with the $\log_{10}A = -14.66 \pm 0.07$ found in Goncharov et al. (2021a). The result of parameter estimation is provided in Figure 1. We note that the maximum a posteriori value of $\sigma_{\log_{10}A}$ differs from zero, which may represent a noise fluctuation.

We checked that the result is robust to the exclusion of three pulsars with particular noise properties: PSRs J0437–4715, J0711–6830, and J1643–1224. PSRs J1643–1224 and J0711–6830 show spin noise with unusual spectral indices and so we consider them population outliers. These two pulsars also do not contribute significantly to the common-spectrum process based on the dropout analysis (Figure 2 in Goncharov et al. 2021a), which is why it is acceptable to exclude them. PSR J0437–4715 shows excess noise that could, in principle, marginally affect the measurement of the common-spectrum process and that does affect the inference of spatial correlations (see the left panel of Figure 3 in Goncharov et al. 2021a).

Additionally, we tested our methodology using simulated data sets. The details of the simulations can be found in Appendix B. One important issue that we identified is that it is essential to include the common-spectrum process in the proposal likelihood, not only in the target likelihood when testing the quasi-common noise hypothesis. If it is excluded, the measurement of $\sigma_{\log_{10}A}$ will always peak at zero, even if data sets were simulated with, e.g., $\sigma_{\log_{10}A} = 2$. This is because the proposal likelihood does not sufficiently match the target likelihood. Non-inclusion of the separate common-spectrum-

¹⁷ We assume a truncated Gaussian distribution because, in reality, our measurements are truncated by uniform prior boundaries that are used to obtain proposal posterior samples.

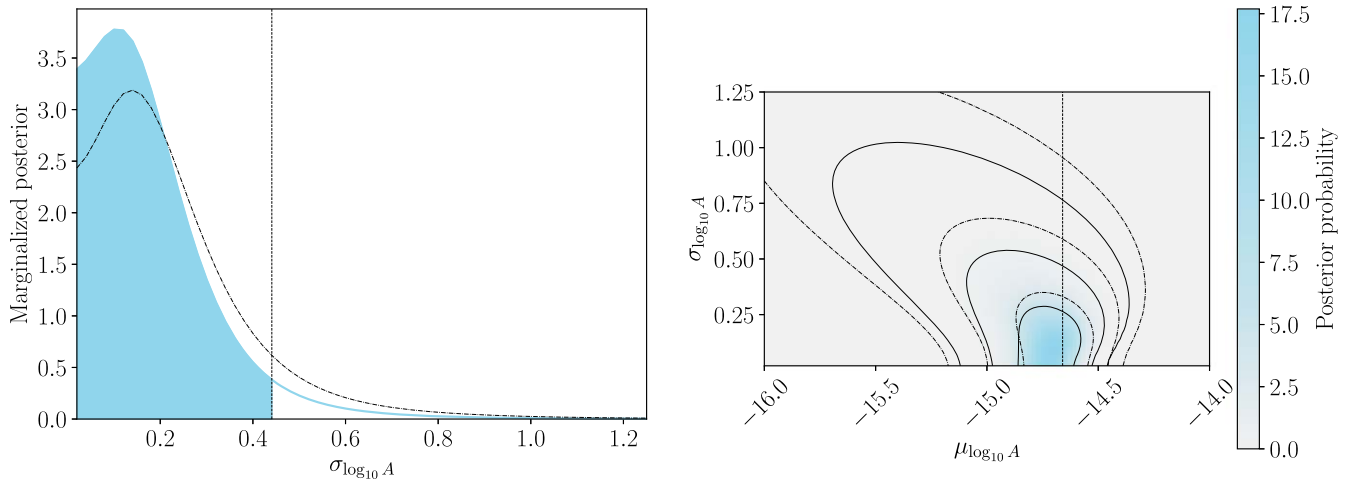


Figure 1. Comparison of common-spectrum and quasi-common-spectrum processes in the PPTA DR2. Left: marginalized posterior for $\sigma_{\log_{10} A}$. The value is consistent with zero, which means that the common-spectrum hypothesis holds for the PPTA data. The vertical dashed line is the upper limit on $\sigma_{\log_{10} A}$ at 95% credibility. Right: full posterior for $\mu_{\log_{10} A}$ and $\sigma_{\log_{10} A}$. The vertical dashed line corresponds to the measurement of $\log_{10} A$ of the common-spectrum process in PPTA DR2 (Goncharov et al. 2021a). Our inference of the common-spectrum-process amplitude is consistent with the previous measurement considering the generalization of the model and the use of likelihood reweighting. Three closed lines correspond to the standard 1σ , 2σ , and 3σ levels. In both panels, the dashed–dotted lines show the measurements performed without three PSRs with special noise properties discussed in Section 3: J0437–4715, J0711–6830, and J1643–1224. Removing these pulsars from the analysis increases uncertainty levels, as expected.

process term will prevent accumulating posterior support in two areas of the parameter space that correspond to the spin noise and the common-spectrum process, respectively. Nevertheless, our methodology is very sensitive to subthreshold red-noise contributions, which is generally true for all Bayesian inference that combines data from multiple measurements (e.g., Goncharov et al. 2020). In particular, even though two power-law processes—(quasi-)common-spectrum process and pulsar-intrinsic spin noise—are not individually resolved in single pulsars, Bayesian inference with the total data set distinguishes them when models match the simulation.

4. Conclusions

We have shown that a pulsar timing array data set, in our case, PPTA DR2, contains a red process that has spectra consistent with stochastic time-series realizations with the single power-law amplitude by measuring σ_A consistent with zero. Note, this conclusion is (a) made under the assumption that the red-process power-law index is $13/3$, which is supported by the PPTA data, but (b) not yet applicable to all available PTA data sets. This discrepancy can potentially be resolved through further data combinations, for example by the IPTA. The identified common-spectrum process in the PPTA DR2 could therefore be the spatially uncorrelated component of the stochastic gravitational-wave background. We expect the variance in measured pulsar spectra from spatial correlations of the pulsar term to exceed that from different time-series realizations of the Earth term, and thus the uncertainty in σ_A to be dominated by the pulsar term. A more detailed investigation of the contribution of both terms to σ_A is a subject of a follow-up study.

The methodology of previous nanohertz gravitational-wave searches might have led to identifying a common-spectrum process when none is present in the data (Goncharov et al. 2021a). Specifically, incorrect conclusions can be caused by a mismatch between uniform noise priors on A and γ in the models and the clustering of these parameters in real data. In particular, for the case of a single power-law red-noise term in

pulsars, evidence for the common-spectrum process disappears when the distribution of true parameters of such noise processes matches the Bayesian priors. The demonstration of the above two points is to be provided by A. Zic et al. (2022, in preparation) simulations where the apparent common-spectrum process arises in a variety of scenarios that only contain pulsar-intrinsic spin noise, whereas the spurious emergence of spatial correlations in such data sets is very unlikely. Determining that the identified noise process is quasi-common could either mean that it is not the gravitational-wave background or that the assumed uniform prior distributions for pulsar-intrinsic noise need to be replaced by more realistic priors. The latter may inform about stochastic irregularities in rotational properties of neutron stars and thus about neutron star physics (Melatos & Link 2014).

Neither our test nor any other test will be able to confirm the common-spectrum hypothesis because it is a matter of measuring the width of the distribution, and we would need an infinitely small measurement uncertainty to rule out all σ_A other than zero. Thus, the techniques we introduce allow us to perform a consistency test and infer common noise properties but cannot be used to detect the stochastic background. Once the gravitational-wave background is detectable through spatial correlations, further modeling of the priors of pulsar-intrinsic spin noise with the techniques we outlined will be required to disentangle these terms. Further simulation study will be useful to test the fidelity of the presented methods under different conditions.

We would also like to point out that it is challenging to extend the methodology to allow γ to vary and thus to measure μ_γ and σ_γ simultaneously with μ_A and σ_A because the accuracy of numerical integration on a grid will decline for a higher-dimensional problem and the computational burden will significantly increase. We foresee several other modifications of the outlined methodology. For example, one could model the distribution of common-process amplitudes A linearly (rather than logarithmically), as well as fix the amplitude and fit for the distribution of power-law indices. Moreover, one could apply

our approach to fitting the distribution of pulsar-intrinsic noise amplitudes and power-law indices, which would result in larger σ_A and σ_γ . Furthermore, in the case of finding stronger evidence for quasi-common noise with $\sigma_A > 0$, it is possible to test a range of functional forms outlining the distribution of A other than the Gaussian distribution we have assumed.

From the perspective of future validation of the detection of the stochastic background, the tests we propose are complementary to other work. The dropout analysis in Arzoumanian et al. (2020) is developed to find outliers in the common-spectrum process. Taylor et al. (2013) introduced an interpolant-based modeling for spatial correlations, which is important to ensure that pulsars exhibit precisely the Hellings–Downs correlations and not something else. Johnson et al. (2022) examine a bias from using a finite number of pulsars. Taylor et al. (2022) develop a factorized likelihood approach for cross-validation of measurements between subsets of timing array pulsars. Romero-Shaw et al. (2022) review several other tests to spot incorrectly specified models. Because, as outlined by Goncharov et al. (2021b), the background noise in PTAs is often not white and Gaussian as assumed by current models and simulations, we suggest studying the effect of this noise on gravitational-wave searches.

We thank Matthew Miles, Paul Baker, Stephen Taylor, and Sarah Vigeland for useful comments. This work has been carried out using the Parkes Pulsar Timing Array, which is part of the International Pulsar Timing Array. Murriyang, the Parkes radio telescope is part of the [Australia Telescope](#), which is funded by the Commonwealth Government for operation as a National Facility managed by CSIRO. This paper includes archived data obtained through the CSIRO Data Access Portal (data.csiro.au). B.G. is supported by the Italian Ministry of Education, University and Research within the PRIN 2017 Research Program Framework, No. 2017SYRTCN. R.M.S. acknowledges support through Australian Research Council Future Fellowship FT190100155. Part of this work was undertaken as part of the Australian Research Council Centre of Excellence for Gravitational Wave Discovery (CE170100004). Work at NRL is supported by NASA.

Software: PYPOLYCHORD (Handley et al. 2015), PTMCMCSAMPLER (Ellis & van Haasteren 2019), ENTERPRISE (Ellis et al. 2019), BILBY (Ashton et al. 2019), github.com/bvgoncharov/enterprise_warp, https://github.com/bvgoncharov/ppta_dr2_noise_analysis.

Appendix A Notes on Data and Analysis

We emphasize that the sources of noise, especially the red-noise terms, should be modeled to ensure the correctness of the analysis. The second data release of the PPTA contains several sources of red noise, which were found and identified in Goncharov et al. (2021b) based on their attribution to the telescope band or system as well as on their radio frequency dependence. Goncharov et al. (2021b) also identified nonstationary sources of noise that affect red noise measurements if not modeled. Incorrect modeling of pulsar timing model parameters such as spin frequency derivatives or instrumental phase jumps can also appear as red noise. Pulsar timing models for PPTA DR2 in coordination with the noise analysis were performed by Reardon et al. (2021). The data set and the code

are available at github.com/bvgoncharov/ppta_dr2_noise_analysis.

Parameter estimation and Bayesian evidence evaluation for individual pulsars are performed with nested sampling (Skilling 2006) implemented in PYPOLYCHORD by Handley et al. (2015). White noise parameter estimation is performed with the PTMCMCSAMPLER (Ellis & van Haasteren 2019). Pulsar likelihoods are modeled using the code ENTERPRISE (Ellis et al. 2019) and linked to PYPOLYCHORD with BILBY (Ashton et al. 2019), using the code available at github.com/bvgoncharov/enterprise_warp.

Appendix B Validating the General Quasi-common-noise Model

We performed a study using a simulated data set to confirm the validity of the importance sampling method as well as the quasi-common-spectrum-process model, for which the common-spectrum process is a limiting case. We note that the common-spectrum-process hypothesis for a given pulsar is described by a likelihood from Equation (2), approximated with the importance sampling by Equation (3). This likelihood is then generalized in Equation (4) to represent the quasi-common-spectrum-process hypothesis.

We simulated a data set with 26 pulsars, as in PPTA DR2, observed for 2555 days, with the pulse arrival time errors of $\sigma_{\text{ToA}} = 0.1 \mu\text{s}$ and the white noise with variance proportional to σ_{ToA} . We then simulate two red-noise processes described by $\log_{10} A$ and γ , as we expect from the stochastic gravitational-wave background and pulsar noise. The simulations are based on 30 frequencies, which correspond to the Fourier basis to model red noise in previous analyses. One red-noise process for each pulsar is drawn from the truncated Normal distribution $\mathcal{N}(\mu, \sigma)$ with $\mu_{\log_{10} A} = -16.3$, $\mu_\gamma = 5$, $\sigma_{\log_{10} A} = 2$, $\sigma_\gamma = 2$. Another red-noise process, the quasi-common noise, has a fixed $\gamma = 13/3$, and $\log_{10} A$ is drawn from the truncated Normal distribution with $\mu_{\log_{10} A} = -13.3$ and $\sigma_{\log_{10} A} = 0.5$. Both Normal distributions are truncated to the edges of the uniform priors used in Goncharov et al. (2021a) to avoid edge effects. The values were chosen so that the pulsar-intrinsic red noise was below the detection threshold of some pulsars, as in PPTA DR2 where only 9 pulsars of 26 show evidence for spin noise. Moreover, quasi-common-noise realizations have simulated A of the order of 10^{-14} – 10^{-13} , as six realizations of the spin noise. The same number of pulsars in PPTA DR2 has the inferred common-process amplitude and the spin-noise amplitude of the same order of magnitude. The results of parameter estimation on the simulated data set are presented in Figure 2. Both the $\mu_{\log_{10} A}$ and the $\sigma_{\log_{10} A}$ are consistent with the simulated values. Note, we tested that this data set shows strong evidence for the common-spectrum process when using the priors from Goncharov et al. (2021a), and yet with our new generalized model, we correctly infer that it is not the case because $\sigma_{\log_{10} A} \neq 0$. More precisely, we find $\log \mathcal{B}_{\emptyset}^{\text{CP}} > 13.5$, where \emptyset is the noise-only null hypothesis that includes only white and red noise, as per the simulations.

The noise in real data is more sophisticated than in the simulations, but it is not necessary to represent the whole complexity of the data to demonstrate the validity of the approach. We defer exhaustive tests of the methodology to future work. Our method is applicable to any data set assuming that physically relevant red-noise processes (from interstellar propagation effects, instrumental noise, etc.) are separated from

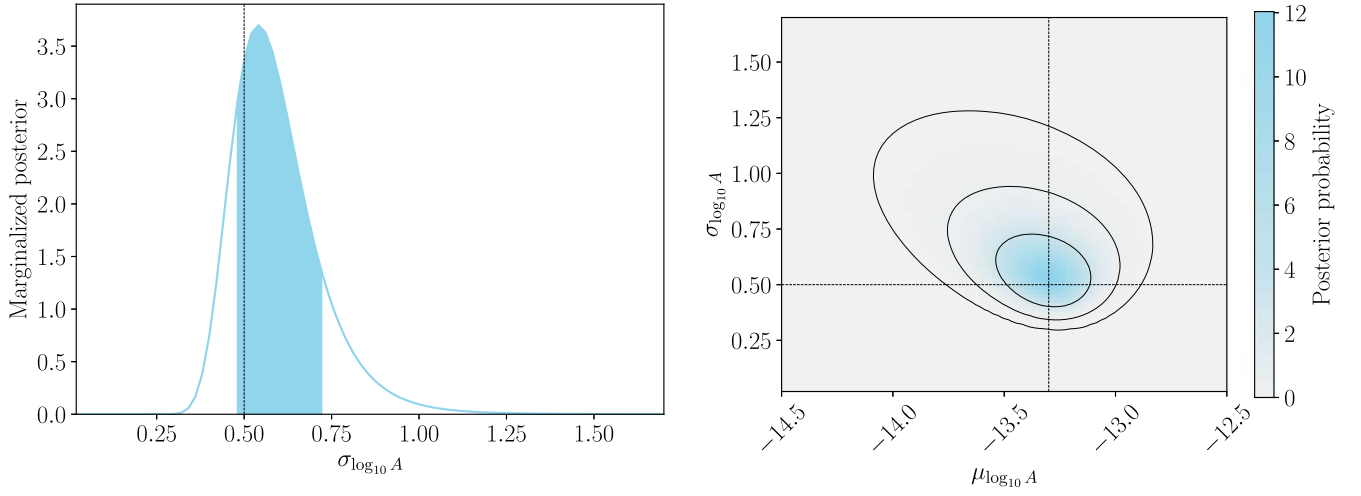


Figure 2. Searches for a quasi-common-spectrum process in a simulated data set. Left: marginalized posterior for $\sigma_{\log_{10} A}$. The value is inconsistent with zero, which means that the signal that would have been interpreted as the common-spectrum process with the standard methods is only a quasi-common-spectrum process. Based on this result, the gravitational-wave origin of the signal can be ruled out. The simulated value is represented by the vertical dotted line and cumulative 1σ credible levels are represented by a shaded region. Right: full posterior on $\mu_{\log_{10} A}$ and $\sigma_{\log_{10} A}$. The vertical and the horizontal lines correspond to the simulated values. Three closed lines correspond to the standard 1σ , 2σ , and 3σ levels.

the common-spectrum process by including them in the models. Moreover, we also find that the current simulation study is robust to the choice of priors for pulsar-intrinsic noise, with the only caveat being that the proposal likelihood should include all red-noise terms in pulsars to allow parameters of both processes to be sampled. We tested that the simulation works for a reduced case with only one red-noise process per pulsar, correctly recovering the position and width of a Gaussian distribution of pulsar red-noise parameters. We also trialed it for the case where the maximum probability densities of the distributions of pulsar spin-noise amplitudes ($\mu_{\log_{10} A} = -14.3$, $\sigma_{\log_{10} A} = 1.3$) and quasi-common-noise amplitudes ($\mu_{\log_{10} A} = -13.8$, $\sigma_{\log_{10} A} = 0.4$) are similar and the distributions have a broader overlap.

Appendix C

Derivation of the Quasi-common-process Likelihood

Whereas Equation (2) models contributions from the common-spectrum process to be represented by one A_c in all pulsars, we can generalize it to model different A_c in pulsars. This way, assuming fixed γ , Equation (2) transforms into

$$\mathcal{L}(\mathbf{d}|\boldsymbol{\theta}, A_{c,1}, \dots, A_{c,N}) = \prod_{k=1}^N \mathcal{L}(\mathbf{d}_k|\boldsymbol{\theta}_k, A_{c,k}). \quad (\text{C1})$$

Marginalizing over all possible values of $A_{c,k}$ in pulsars over the prior distribution these parameters are drawn from, which we model as a Gaussian distribution with μ and σ , the likelihood becomes

$$\begin{aligned} \mathcal{L}(\mathbf{d}|\boldsymbol{\theta}, \mu, \sigma) &= \prod_{k=1}^N \mathcal{L}(\mathbf{d}_k|\boldsymbol{\theta}_k, \mu, \sigma) \\ &= \prod_{k=1}^N \int \mathcal{L}(\mathbf{d}_k|\boldsymbol{\theta}_k, A_{c,k}) \pi(A_{c,k}|\mu, \sigma) dA_{c,k}. \end{aligned} \quad (\text{C2})$$

Next, let us marginalize over the “nuisance” parameters $\boldsymbol{\theta}$,

$$\mathcal{L}(\mathbf{d}|\mu, \sigma) = \prod_{k=1}^N \int \mathcal{L}(\mathbf{d}_k|\boldsymbol{\theta}_k, \mu, \sigma) \pi(\boldsymbol{\theta}_k) d\boldsymbol{\theta}_k. \quad (\text{C3})$$

Let us then multiply the equation by unity and expand the unity via the proposal likelihood $\mathcal{L}(\mathbf{d}_k|\boldsymbol{\theta}_k)$,

$$\mathcal{L}(\mathbf{d}|\mu, \sigma) = \prod_{k=1}^N \int \frac{\mathcal{L}(\mathbf{d}_k|\boldsymbol{\theta}_k)}{\mathcal{L}(\mathbf{d}_k|\boldsymbol{\theta}_k)} \mathcal{L}(\mathbf{d}_k|\boldsymbol{\theta}_k, \mu, \sigma) \pi(\boldsymbol{\theta}_k) d\boldsymbol{\theta}_k. \quad (\text{C4})$$

Representing one proposal likelihood through the posterior $\mathcal{P}(\boldsymbol{\theta}_k|\mathbf{d}_k)$, the evidence $\mathcal{Z}(\mathbf{d}_k)$, and the prior $\pi(\boldsymbol{\theta}_k)$, we obtain

$$\mathcal{L}(\mathbf{d}|\mu, \sigma) = \prod_{k=1}^N \int \mathcal{Z}(\mathbf{d}_k) \mathcal{P}(\boldsymbol{\theta}_k|\mathbf{d}_k) \left(\frac{\mathcal{L}(\mathbf{d}_k|\boldsymbol{\theta}_k, \mu, \sigma)}{\mathcal{L}(\mathbf{d}_k|\boldsymbol{\theta}_k)} \right) d\boldsymbol{\theta}_k, \quad (\text{C5})$$

where the prior canceled out. Next, we approximate the integral for a k th pulsar with a sum over n_k posterior samples, $\boldsymbol{\theta}_{k,j}$, providing

$$\mathcal{L}(\mathbf{d}|\mu, \sigma) = \prod_{k=1}^N \mathcal{Z}(\mathbf{d}_k) \frac{1}{n_k} \sum_{j=1}^{n_k} \frac{\mathcal{L}(\mathbf{d}_k|\boldsymbol{\theta}_{k,j}, \mu, \sigma)}{\mathcal{L}(\mathbf{d}_k|\boldsymbol{\theta}_{k,j})}, \quad (\text{C6})$$

where, omitting $\boldsymbol{\theta}_{k,j}$,

$$\mathcal{L}(\mathbf{d}_k|\mu, \sigma) = \int \mathcal{L}(\mathbf{d}_k|A_{c,k}) \pi(A_{c,k}|\mu, \sigma) dA_{c,k}. \quad (\text{C7})$$

The approximation of an integral via the sum of posterior samples is explained for various applications in Hogg & Foreman-Mackey (2018) and Thrane & Talbot (2019).

ORCID iDs

Boris Goncharov <https://orcid.org/0000-0003-3189-5807>
Eric Thrane <https://orcid.org/0000-0002-4418-3895>
Ryan M. Shannon <https://orcid.org/0000-0002-7285-6348>
Jan Harms <https://orcid.org/0000-0002-7332-9806>
N. D. Ramesh Bhat <https://orcid.org/0000-0002-8383-5059>
Matthew Kerr <https://orcid.org/0000-0002-0893-4073>

Richard N. Manchester  <https://orcid.org/0000-0001-9445-5732>
 Daniel J. Reardon  <https://orcid.org/0000-0002-2035-4688>
 Christopher J. Russell  <https://orcid.org/0000-0002-1942-7296>
 Xing-Jiang Zhu  <https://orcid.org/0000-0001-7049-6468>
 Andrew Zic  <https://orcid.org/0000-0002-9583-2947>

References

- Antoniadis, J., Arzoumanian, Z., Babak, S., et al. 2022, *MNRAS*, **510**, 4873
 Arzoumanian, Z., Baker, P. T., Blumer, H., et al. 2020, *ApJL*, **905**, L34
 Arzoumanian, Z., Brazier, A., Burke-Spolaor, S., et al. 2016, *ApJ*, **821**, 13
 Ashton, G., Hübner, M., Lasky, P. D., et al. 2019, *ApJS*, **241**, 27
 Caballero, R. N., Lee, K. J., Lentati, L., et al. 2016, *MNRAS*, **457**, 4421
 Casey-Clyde, J. A., Mingarelli, C. M. F., Greene, J. E., et al. 2022, *ApJ*, **924**, 93
 Chalumeau, A., Babak, S., Petiteau, A., et al. 2022, *MNRAS*, **509**, 5538
 Chen, S., Caballero, R. N., Guo, Y. J., et al. 2021, *MNRAS*, **508**, 4970
 Desvignes, G., Caballero, R. N., Lentati, L., et al. 2016, *MNRAS*, **458**, 3341
 Dickey, J. M. 1971, *Ann. Math. Stat.*, **42**, 204
 Edwards, R. T., Hobbs, G. B., & Manchester, R. N. 2006, *MNRAS*, **372**, 1549
 Ellis, J., & van Haasteren, R. 2019, PTMCMCSampler: Parallel tempering MCMC sampler package written in Python, Astrophysics Source Code Library, ascl:1912.017
 Ellis, J. A., Vallisneri, M., Taylor, S. R., & Baker, P. T. 2019, ENTERPRISE: Enhanced Numerical Toolbox Enabling a Robust Pulsar Inference Suite, Astrophysics Source Code Library, ascl:1912.015
 Gelman, A., Carlin, J. B., Stern, H. S., & Rubin, D. B. 1995, *Bayesian Data Analysis* (2nd ed.; London: Chapman and Hall)
 Goncharov, B., Reardon, D. J., Shannon, R. M., et al. 2021b, *MNRAS*, **502**, 478
 Goncharov, B., Shannon, R. M., Reardon, D. J., et al. 2021a, *ApJL*, **917**, L19
 Goncharov, B., Zhu, X.-J., & Thrane, E. 2020, *MNRAS*, **497**, 3264
 Handley, W. J., Hobson, M. P., & Lasenby, A. N. 2015, *MNRAS*, **453**, 4384
 Hellings, R. W., & Downs, G. S. 1983, *ApJL*, **265**, L39
 Hogg, D. W., & Foreman-Mackey, D. 2018, *ApJS*, **236**, 11
 Izquierdo-Villalba, D., Sesana, A., Bonoli, S., & Colpi, M. 2022, *MNRAS*, **509**, 3488
 Johnson, A. D., Vigeland, S. J., Siemens, X., & Taylor, S. R. 2022, arXiv:2201.10657
 Kerr, M., Reardon, D. J., Hobbs, G., et al. 2020, *PASA*, **37**, e020
 Lentati, L., Alexander, P., Hobson, M. P., et al. 2014, *MNRAS*, **437**, 3004
 Lentati, L., Shannon, R. M., Coles, W. A., et al. 2016, *MNRAS*, **458**, 2161
 Manchester, R. N., Hobbs, G., Bailes, M., et al. 2013, *PASA*, **30**, e017
 McLaughlin, M. A. 2013, *CQGra*, **30**, 224008
 Melatos, A., & Link, B. 2014, *MNRAS*, **437**, 21
 Meyers, P. M., O'Neill, N. J., Melatos, A., & Evans, R. J. 2021, *MNRAS*, **506**, 3349
 Payne, E., Talbot, C., & Thrane, E. 2019, *PhRvD*, **100**, 123017
 Pol, N. S., Taylor, S. R., Kelley, L. Z., et al. 2021, *ApJL*, **911**, L34
 Reardon, D. J., Shannon, R. M., Cameron, A. D., et al. 2021, *MNRAS*, **507**, 2137
 Renzini, A. I., Goncharov, B., Jenkins, A. C., & Meyers, P. M. 2022, *Galax*, **10**, 34
 Romano, J. D., Hazboun, J. S., Siemens, X., & Archibald, A. M. 2021, *PhRvD*, **103**, 063027
 Romero-Shaw, I. M., Thrane, E., & Lasky, P. D. 2022, *PASA*, **39**, e025
 Shannon, R. M., & Cordes, J. M. 2010, *ApJ*, **725**, 1607
 Skilling, J. 2006, *BayAn*, **1**, 833
 Taylor, S. R., Gair, J. R., & Lentati, L. 2013, *PhRvD*, **87**, 044035
 Taylor, S. R., Lentati, L., Babak, S., et al. 2017, *PhRvD*, **95**, 042002
 Taylor, S. R., Simon, J., Schult, L., Pol, N., & Lamb, W. G. 2022, *PhRvD*, **105**, 084049
 Thrane, E., & Talbot, C. 2019, *PASA*, **36**, e010
 van Haasteren, R., Levin, Y., McDonald, P., & Lu, T. 2009, *MNRAS*, **395**, 1005
 Verbiest, J. P. W., Lentati, L., Hobbs, G., et al. 2016, *MNRAS*, **458**, 1267